Original paper

Cardiac contraction motion compensation in gated myocardial perfusion SPECT: A comparative study

Narges Salehi[a,b], Arman Rahmim[c,d], Emad Fatemizadeh[e], Afshin Akbarzadeh[b],
Mohammad Hossein Farahani[b], Saeed Farzanefar[f], Mohammad Reza Ay[a,b,*]

[a] Department of Medical Physics and Biomedical engineering, School of Medicine, Tehran University of Medical Science, Tehran, Iran
[b] Research Center for Molecular and Cellular Imaging, Tehran University of Medical Sciences, Tehran, Iran
[c] Department of Radiology, Johns Hopkins University, Baltimore, MD, USA
[d] Department of Electrical & Computer Engineering, Johns Hopkins University, Baltimore, MD, USA
[e] Electrical Engineering Department, Sharif University of Technology, Tehran, Iran
[f] Department of Nuclear Medicine, Vali-Asr Hospital, Tehran University of Medical Sciences, Tehran, Iran

ARTICLE INFO

ABSTRACT

Introduction: Cardiac contraction significantly degrades quality and quantitative accuracy of gated myocardial perfusion SPECT (MPS) images. In this study, we aimed to explore different techniques in motion-compensated temporal processing of MPS images and their impact on image quality and quantitative accuracy.

Material and method: 50 patients without known heart condition underwent gated MPS. 3D motion compensation methods using Motion Freezing by Cedars Sinai (MF), Log-domain Diffeomorphic Demons (LDD) and Free-Form Deformation (FFD) were applied to warp all image phases to fit the end-diastolic (ED) phase. Afterwards, myocardial wall thickness, myocardial to blood pool contrast, and image contrast-to noise ratio (CNR) were measured in summed images with no motion compensation (NoMC) and compensated images (MF, LDD and FFD). Total Perfusion Defect (TPD) was derived from Cedars-Sinai software, on the basis of sex-specific normal limits.

Result: Left ventricle (LV) lateral wall thickness was reduced after applying motion compensation ($p < 0.05$). Myocardial to blood pool contrast and CNR in compensated images were greater than NoMC ($p < 0.05$). TPD_LDD was in good agreement with the corresponding TPD_MF ($p = 0.13$).

Conclusion: All methods have improved image quality and quantitative performance relative to NoMC. LDD and FFD are fully automatic and do not require any manual intervention, while MF is dependent on contour definition. In terms of diagnostic parameters LDD is in good agreement with MF which is a clinically accepted method. Further investigation along with diagnostic reference standards, in order to specify diagnostic value of each technique is recommended.

1. Introduction

Single photon emission computed tomography (SPECT) imaging provides an effective, non-invasive framework to assess myocardial perfusion [1]. Myocardial perfusion SPECT (MPS) images suffer from several degradation factors, the most important factors being cardiac and respiratory motion which cause artifacts and spatial blurring in the MPS images [2]. Respiratory motion is more or less locally rigid, while cardiac motion is highly non-rigid [3,4]. The myocardial wall moves relative to the detectors; therefore, acquired data are blurred and image resolution is degraded [5]. Mean myocardial motion during a cardiac cycle has been reported to be 12–13 mm, with endocardial motion ranging between end-diastolic (ED) and end-systolic (ES) frames reported as $13 \pm 2\, mm$ and $14 \pm 2\, mm$ for males and females, respectively, and $12 \pm 2\, mm$ for both genders in epicardial displacement [6,7]. A suitable method to overcome motion blurring is to use gating for separating the emission data into cardiac (and/or respiratory) phases [8]. Although gating reduces motion in each time frame, noise level will be elevated due to low count density at each time bin [3]. As long as gated image frames are noisy, accurate quantification is impossible; therefore, these gates are summed together and the summed image is used to study myocardial perfusion [9]. Several studies have illustrated that in patients with small heart size, sensitivity increases when using selected end-diastolic (ED) frames for the visual assessment

---

of MPS [10]. Since motion-induced image blurring has a significant effect on quantification results, summed image quantification results may not be reliable. On the other hand, quantification results for the ED frame are not optimal, due to lower count density and noise [7,10]. Another significant factor causing quantification inaccuracy is the signal cross-contamination between the blood pool (cardiac chamber) and normal myocardial tissue in small sized hearts, due to limited resolution of the imaging system [11]. Several studies have been conducted on motion estimation and compensation. These methods can be broadly classified into two categories: averaging of aligned post-reconstruction images and reconstruction-based compensation for motion [2–4,6,7,11–21]. Reconstruction-based methods require access to the raw data and specific image reconstruction platform for a given scanner. By contrast, post-reconstruction methods are potentially amenable to wider dissemination in clinical practice. In the present work, we study and evaluate post-reconstruction methods to overcome motion-induced blurring in gated MPS, so as to improve the image quality and increase diagnostic value of the images.

2. Materials and method

2.1. Clinical acquisition protocol

Patient Population: Myocardial perfusion SPECT data in our department were used retrospectively. 50 low risk patients with normal presentation of myocardial perfusion images with End Systolic Volume (ESV) ≤ 20 ml, who had undergone their stress MPI by ADAC-Forte gamma Camera (Philips Medical Systems, North Milpitas, CA, USA) and 18 patients were imaged using RoboSPECT dedicated cardiac Gamma camera (Parto Negar Persia (PNP) co, Tehran, Iran), were selected by Nuclear medicine specialist (41 female and 9 male; 30–87 years (58.76 ± 12.4); Body Mass Index (BMI) of 30.1–46.8). The subjects underwent standard supine rest and stress Tc-99 m-sestamibi gated MPS. Prior to data acquisition, patients underwent either exercise or adenosine stress protocols as described in Ref. [9]. MPS acquisitions were performed using noncircular orbits and 32 projections over 180 degrees (45 right anterior oblique to 45 left posterior oblique) at 25 s/ projection for Tc-99 m-sestamibi. All images were subject to standard clinical quality-control measures [9].

All stress scans were reconstructed using filtered back-projection with a Butterworth filter (cutoff: 0.4 cycle/mm, order: 10 for the gated projections). After reconstruction of gated data with filtered back projection (FBP), short-axis slices were automatically generated. Iterative ordered-subset expectation–maximization reconstruction was performed for non-motion compensated Summed (NoMC) perfusion data [22]. All the data were anonymized prior being used for study using MATLAB. All the MATLAB codes were written and performed on a PC (64-bit operating system, Processor: Core i7-6700 CPU @ 3.40 GHz 3.20 GHz, RAM: 8 GB) and the computer used for medical analysis using QPS-QGS Cedars_Sinai software, PC (Processor: Core i5-3330 CPU @ 3.00 GHz 3.20 GHz, RAM: 8 GB, Graphic Card: Geforce GT 630 (NVIDIA)).

2.2. Motion compensation methods

Our experimental set up was inspired by the research conducted by Slomka,et al. and Kovalski, et al., in [7] and [6], respectively. In the aforementioned studies, motion compensation in MPS is treated as a non-rigid landmark-based registration problem. The technique introduced in [7] is known as Motion Freezing which has been implemented clinical in the Cedars-Sinai software package. In this study we have utilized two different registration algorithms in order to find a non-rigid summation of different time frames of MPS. Log-Diffeomorphic Demons (LDD) and Free Form Deformation (FFD), have been chosen as an alternatives to the conventional land-mark based registration solutions, and are discussed as below.

These approaches require the following steps: 1) Computing deformation maps for each 3D cardiac SPECT volume with respect to the reference in the 4D series which is ED frame; 2) Use the deformation maps computed in Step 1 to warp each volume to the ED volume; 3) Average the registered volumes to generate a single motion-compensated summed image [23].

2.2.1. Motion freezing

This technique is one of the features in Quantitative Perfusion SPECT (QPS) application of the Cedars-Sinai software, which employs a novel technique to create cardiac "motion-frozen" perfusion or viability images by warping all frames of ECG-gated images to the end-diastolic position. It compensates for motion by tracking *endo*-cardial and epicardial motions. The epi- and endocardial points are detected in each interval along vectors that are normal to the mid-myocardial points; by fitting an asymmetric Gaussian function to their respective count profiles, following this step each cardiac frame is warped with respect to the ED-frame by the 3D Thin Plate Spline algorithm. Such "motion frozen" perfusion and viability images improve resolution and contrast, as the blurring effect of cardiac motion is removed. And no manual intervention was performed in the derivation of the MF results and no failures of the contour detection were observed [7].

2.2.2. Log-domain Diffeomorphic Demons (LDD)

Symmetric Log-domain Diffeomorphic Demons (LDD) is an efficient algorithm due to use of demons-like alternate optimization while representing deformation as an exponential of a smooth velocity field. The key concept behind this algorithm is finding the optimal transformation field, by computing the correspondence update field via diffeomorphic demons [24]. A diffeomorphic transformation (φ), $\varphi: \Omega \to \Omega, \Omega \subset \mathbb{R}^d$ is a globally one-to-one and differentiable mapping from space Ω to Ω (where Ω is in a d dimensional real space), with a differentiable inverse, so that it is topology preserving with respect to the structures. Smoothness preservation of anatomical features is imposed to maintain connectivity between structures (i.e. being diffeomorphic), a consideration commonly applied in medical image registration [25]. We have 7 volumetric non-diastolic frames that need to be warped to ED volume; these frames form our moving images $M(x)$ and ED-frame is the fixed image $F(x)$, each defined in their own spatial domain, $\Omega_M \subset \mathbb{R}^d$ and $\Omega_F \subset \mathbb{R}^d$, respectively. During registration, we try to find a transformation that will align non-diastolic frames to the ED frame [23,24]. The energy functional is as follows [26]:

$$E(v,v_c) = \left\| \frac{1}{\sigma_i^2}(F-M \circ \exp(v_c))^2 \right\| + \frac{1}{\sigma_x^2} \|\log(\exp(-v) \circ \exp(v_c))\|^2 + \frac{1}{\sigma_T^2}\|\nabla v\|^2 \tag{1}$$

where F stands for Fixed (reference) image which in our case is the ED-frame and M is the moving image (non-ED frames), σ_i^2 is related to the image noise, σ_x^2 controls regularization, v is the velocity field and v_c parameterizes the transformation modeling the correspondences between voxels of F and M.

An initial stationary velocity field v_0 and spatial transformation s = exp (v_0) is defined, and the algorithm iterates until meeting the stopping criteria which is energy functional minimization. The algorithm steps are as follows:

- Velocity field v is computed with respect to former field v_0 The space of velocities is in the log-domain
- A fluid like regularization using Gaussian kernel is performed on the velocity field v
- The velocity between correspondence voxels is computed v_c
- Diffusion-like regularization using Gaussian kernel is performed on the velocity field $v \leftarrow Gaussian*v_c$
- M is warped: $M \circ s = M \circ exp(v)$

- Repeat until the energy function is minimized

2.2.3. Free Form Deformation (FFD)

Rueckert et al. [27] proposed a method which consists of two step (Eq. (2)). First step is estimation of an affine transformation so as to establish an initial alignment between ED-frame and Non-ED frames. In the next step, the local deformations are modeled by B-spline methodology [28], enabling definition of an efficient local transformation, since the displacement of a point is only affected by the neighboring grid points. As it is obvious, altering the points significantly impacts the local transformation [29]. This technique consists of two step (Eq. (2)): A global transformation $T_{global}(x,y,z)$ which is considered an affine transformation in this study, and has 12 degrees of freedom as described in [27] and is parameterized by coefficient θ, and a local transformation $T_{local}(x,y,z)$ which is the B-spline is illustrated in Eq. (3).

$$T(x,y,z) = T_{global}(x,y,z) + T_{local}(x,y,z) \tag{2}$$

As stated in [27], local motion model is assumed as below: Image volume domain is denoted as $\Omega = \{(x,y,z) | 0 \leqslant x < X, 0 \leqslant y < Y, 0 \leqslant z < Z\}$. And Φ is a mesh of $n_x \times n_y \times n_z$ of control points, where all points $(\varphi_{i,j,k})$ have uniform spacing δ with respect to one another [27].

$$T_{local}(x,y,z) = \sum_{l=0}^{3} \sum_{m=0}^{3} \sum_{n=0}^{3} B_l(u)B_m(v)B_n(w)\varphi_{i+l,j+m,k+n} \tag{3}$$

Where $i = \lfloor x/n_x \rfloor - 1$, $j = \lfloor y/n_y \rfloor - 1$, $k = \lfloor z/n_z \rfloor - 1$, $u = x/n_x - \lfloor x/n_x \rfloor$, $v = y/n_y - \lfloor y/n_y \rfloor$, $w = z/n_z - \lfloor z/n_z \rfloor$ and B_l represents lth basis function of the B-spline: (see [27]).

$$B_0(u) = \frac{(1-u)^3}{6}$$

$$B_1(u) = \frac{3u^3 - 6u^2 + 4}{6}$$

$$B_2(u) = \frac{-3u^3 + 3u^2 + 3u + 1}{6}$$

$$B_3(u) = \frac{u^3}{6}$$

This functional is solved as an optimization problem, which minimizes a cost function incorporated from global and local transformation parameters (Eq. (4)).

$$C(\theta,\varphi) = -C_{similarity}(I(t_0),T(I(t))) + \lambda C_{smooth} \tag{4}$$

Where λ is a weighting parameter used to define a tradeoff between alignment of two image volumes and smoothness [27]. In this study similarity index used is Sum Squared Distance (SSD) as this measure has been used in LDD algorithm, too.

2.3. Performance evaluation

2.3.1. Jacobian Map

To evaluate physical plausibility of deformation, we examined the singularities in both LDD and FFD methods, as we had the deformation fields. A deformation must be one-to-one or bijective which uniquely maps points in both fixed and moving images to each other and therefore, regions where the deformation field is not one-to-one are referred to as singularities. To do this, we calculated the determinant of the Jacobian of the deformation field at every point. Each point with Jacobian $\leqslant 0$ denotes a singularity [30].

2.3.2. Signal to Noise Ratio (SNR), Contrast to Noise Ratio (CNR) and Myocardium to Blood Pool (M/BP) Contrast

LV and blood pool volumes of interests (VOIs) were generated. Mean and standard deviation (σ) values of VOIs were calculated for each data set for both myocardium and blood pool. The following metrics were calculated.

$$SNR = \frac{\mu_{LV}}{\sigma_{blood}} \tag{5}$$

$$CNR = \frac{\mu_{LV} - \mu_{blood}}{\sigma_{blood}} \tag{6}$$

$$Myocardium\ to\ blood\ contrast = \frac{\mu_{LV} - \mu_{blood}}{\mu_{LV} + \mu_{blood}} \tag{7}$$

where μ_{LV} and μ_{blood} are the mean number of counts in the left ventricle myocardium and blood pool, respectively, and σ_{blood} is the standard deviation of count in blood pool [31].

2.3.3. Myocardial wall thickness

Three consecutive middle slices were selected from end diastolic frame and end-systolic frame before and after motion compensation to reduce noise influence and the average wall thickness was calculated [32]. Line profiles were taken across the lateral wall of the left ventricle which has the largest motion [11,32]. A Gaussian curve was fitted on the line profiles and the FWHM of the fitting function was used [2].

2.3.4. Total Perfusion Deficit (TPD)and Segmental Scores(Bullseye map)

TPD and Bullseye maps (20 segments, AHA) of Non-Motion-compensated (NoMC) and compensated summed images were automatically derived and calculated on the basis of sex specific normal limits obtained from the healthy population using the Cedars-Sinai software [33].

2.4. Statistical analysis

All statistical analyses were performed using SPSS Statistics version 21 (Armonk, NY: IBM Corp) and MedCalc version 12.1.4.0 (Belgium). All continuous variables are expressed as mean ± SD. Analysis of Variance (ANOVA), Paired-T tests were used to compare differences in paired continuous normally distributed data, and the Wilcoxon rank sum test was used for non-normally distributed data. And Pearson correlation coefficients were computed. All statistical tests were 2-tailed, and a p-value of < 0.05 was considered significant.

3. Results

3.1. Jacobian map

The Jacobian determinant contains information regarding the bijectivity of the mapping, and when it is greater than zero, it ensures the topology preserving mapping property of the algorithm. The Jacobian map of deformation field vectors were computed for each patient and then averaged over the 50 patients. The determinant value for LDD and FFD motion fields were 1.05 ± 0.12 and 1.02 ± 0.10, respectively. None of the voxels demonstrated any singularity, indicating that deformations were plausible [30].

3.2. SNR, myocardium to blood pool contrast and CNR

There was a not a significant effect of motion compensation on Signal to Noise Ratio (SNR) at the $p < 0.05$ level for the four conditions [$F(3,196) = 0.59$, $p = 0.61$]. The myocardium-to-blood pool contrast (M/BP Contrast), CNR significantly changed between the NoMC and compensated images (Table 1), ([$F(3,196) = 20.20$, $p < 0.0001$], [$F(3,196) = 25.37$, $p < 0.0001$], respectively. The pairwise comparisons via paired sample t-test are shown in Table 2. Fig. 1 provides CNR results on a per-method basis: CNR of compensated images were significantly different than NoMC images ($p < 0.05$). Examples of improvements in terms of visual image quality before and after motion compensation can be seen in Figs. 2 and 3.

Table 1
Performance measures of images before and after motion compensation by Motion Freezing (MF), Log-domain diffeomorphic demons (LDD), Free Form Deformation (FFD).

Image Type	Image Quality		
	SNR	CNR	Myocardium to Blood pool Contrast (%)
NoMC	5.40 ± 3.65	1.53 ± 0.66	18.9 ± 8.3
MF	5.86 ± 1.65	2.85 ± 0.81	33.2 ± 9.8
LDD	6.19 ± 3.87	2.19 ± 0.76	24.2 ± 8.5
FFD	5.39 ± 4.38	2.03 ± 0.80	27.6 ± 10.7

Table 2
Statistical comparisons between image assessment metrics for different methods.

Statistical difference	CNR (p-value)	CNR (r^2)	M/BP contrast (p-value)	M/BP contrast (r^2)	SNR (p-value)
NoMC/MF	p < 0.0001	0.83	p < 0.0001	0.83	p < 0.0001
NoMC/LDD	p < 0.0001	0.81	P = 0.015	0.87	p = 0.97
NoMC/FFD	p = 0.003	0.77	P < 0.0001	0.84	p = 1
MF/LDD	p < 0.0001	0.78	p < 0.0001	0.88	p = 0.60
MF/FFD	p < 0.0001	0.75	p < 0.0001	0.92	p < 0.0001
LDD/FFD	P = 0.9	0.90	P = 0.19	0.94	p = 0.94

Fig. 1. Contrast to Noise Ratio (CNR) before and after compensation per method basis.

3.3. Summed image lateral wall thickness

Lateral wall thickness in summed and compensated images by MF, LDD and FFD are 3.55 ± 0.40, 3.31 ± 0.5, 3.35 ± 0.42 and 3.35 ± 0.64 mm, respectively. Motion compensation did not significantly alter lateral wall thickness at the p < 0.05 level for the four conditions [F(3,196) = 2.14, p = 0.096]. The results of each paired comparisons using paired sample T-test are shown in Table 3.

3.4. Total perfusion defect (TPD)

We observed a statistically significant difference between TPD values in NoMC (4.92 ± 4.1) vs. MF (7.22 ± 5.06) (p-value = 0.001), MF vs. FFD(11.1 ± 7.5) (p-value = 0.002), and LDD (6.32 ± 4.15) vs. FFD (p-value < 0.0001), as reported in Table 4. The difference of the two paired measurements (TPD-MF and TPD-LDD) is plotted against the mean of the two measurements in the Bland-Altman plot of Fig. 4. Results showed no statistically significant difference between these measurements (p = 0.14), since 95% of the data points lie within ± 2 SD of the mean difference: this agreement can be visually assessed in Fig. 4.

4. Discussion

In this study three motion compensation methods were implemented, which involve non-rigid summation of gated frames to obtain motion induced-blurring free static images.

Motion-Freezing (MF) technique, compensates myocardial motion by tracking endocardial and epicardial movements, by assuming intersection points between mid-myocardial surface and its respective normal vectors, as the control points. Following control point selection, non-ED frames would be warped to ED frame using Thin Plate Spline (TPS) [7]. As TPS warping is facilitated by symmetric logarithmic radial basis functions; therefore, if control points are irregularly placed, large errors might occur for points, which are far from control points [34]. Thus, contour definition plays an important role in MF technique as suggested by Slomka, et al. in [7]. Error in contours causes inaccuracy in quantification and image display, and also in the case of small hearts, where signal is degraded in end-systolic frames due to the partial volume effect, this technique would not be able to define correct control points, and the algorithm cannot be implemented [7]. With respect to the transformation itself, it is worth mentioning that TPS transformations become global, as logarithmic basis functions are monotonically increase to encapsulate all voxels. Therefore, their adaptation to local transformations would become impossible [34,35]. Since MF only takes motion normal to the cardiac surfaces and does not model apical torsion of the heart [15], TPS is not able to compensate local transformations in this area.

Log-Diffeomorphic Demons (LDD) estimates diffeomorphic transformations parameterized by stationary velocity fields [36] and is well adapted to local deformations. But it is dependent on image intensity to some extent. This algorithm assumes the grey level information is
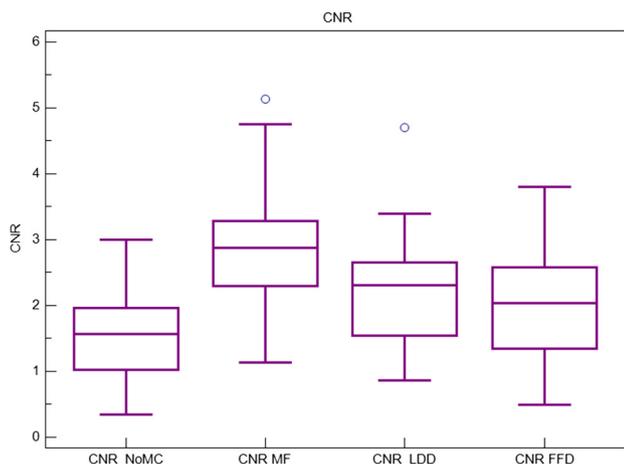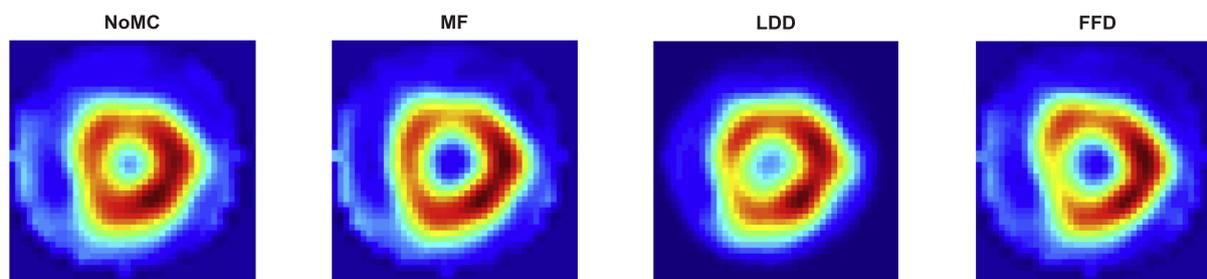

Fig. 2. A 57 years old female patient with low likelihood of CAD and a small sized heart, weight = 68 kg underwent gated stress imaging with Tc-99 mibi, Summed image and Motion-compensated (MF, LDD and FFD) Images.
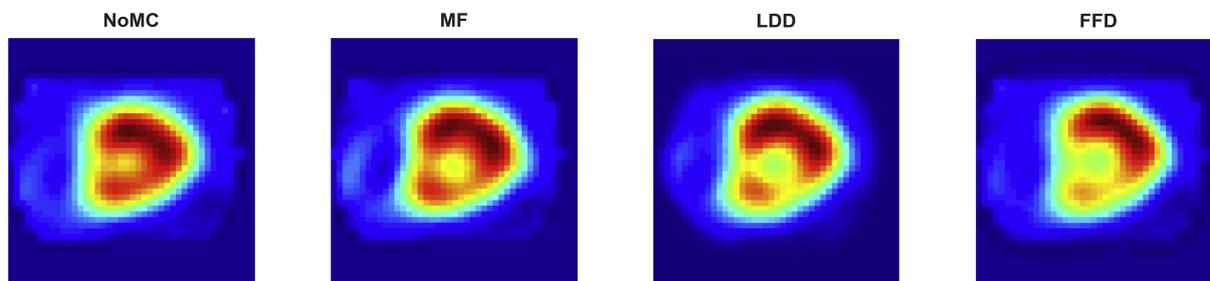
Fig. 3. A 55 years old male patient with low likelihood of CAD, and a very small heart which has lost its resolution in systolic frames, weight = 76 kg underwent gated stress imaging with Tc-99 mibi, Summed image and Motion-compensated (MF, LDD and FFD) Images.

Table 3
Lateral wall thickness in summed images.

Lateral wall thickness	p-value	r²
NoMC/MF	p < 0.0001	0.68
NoMC/LDD	p < 0.0001	0.72
NoMC/FFD	P = 0.02	0.44
MF/LDD	P = 0.05	0.96
MF/FFD	P = 0.05	0.76
LDD/FFD	p = 0.89	0.70

Table 4
Pairwise difference of TPDs.

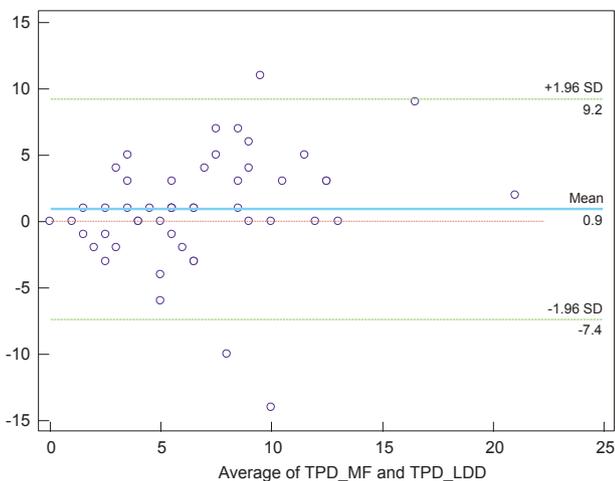| TPDs	p-value
NoMC/MF	0.001
NoMC/LDD	0.23
NoMC/FFD	< 0.0001
MF/LDD	0.14
MF/FFD	0.002
LDD/FFD	< 0.0001

Fig. 4. Bland-Altman plot for comparing resultant TPD of compensated images using MF and LDD.

constant in time frames, whereas corresponding points in frames might have rather variant intensities. This might lead to consistency problem, but it also enforces invertibility and memory efficacy [24,35].

In this study we also implemented FFD image registration which is a combination of affine transformations and B-spline. In this method deformation field is modeled by using B-splines on a regular grid [37]. As it has been demonstrated by Rueckert, et al., this method is flexible in terms of motion modeling in an incompressible tissues [27].

The LDD and FFD algorithm are topology-preserving, which means they produce a mapping which is continuous, and locally one-to-one

and has a continuous inverse and guarantees that connected regions of an image remain connected [38]. The Jacobian determinant for all data was equal to 1.05 ± 0.12 and 1.02 ± 0.10 for LDD and FFD, respectively. This measure reflects how physically plausible the registration deformation is. Regions where the deformation field is not one-to-one are commonly referred to as singularities. Every point with a Jacobian ≤ 0 denotes a singularity [30].

Uniform blurring causes wall thickening effect in Non-motion-compensated (NoMC) summed images [6,7,39]. In this study we evaluated lateral wall thickness as an indicator of motion compensation impact on wall thickness, as lateral wall has the largest motion in heart muscle [11]. Results from the study conducted by Petibon et al. indicated that the contrast of the "lateral" wall also benefits from motion compensation [11]. As shown in Table 3, lateral wall thickness differs significantly from that in non-motion-compensated images (p < 0.0001) and there is no statistically significant difference between wall thickness in MF and LDD images and are strongly correlated.

The Limited spatial resolution of imaging systems might result in count spill-over, since blood pool and defects are prone to signal spill-over due to cardiac motion and the partial volume effect; therefore, contrast degradation is conspicuous between myocardium/blood pool and myocardium/defect contrast [11]. In the systolic frames, the cardiac blood pool is smaller and the LV walls seem thicker due to the LV myocardial contraction. The effect of blurring is therefore more pronounced in the end-systolic frames than in the end-diastolic frames, with a reduced myocardium-to-blood contrast, poorer quantitative accuracy, and degraded image quality overall [11,40]. Importantly, as shown in Tables 1 and 2, the myocardium-to-blood contrast is significantly improved with motion compensation by all three methods, with no reduction in the SNR or CNR.

Although, apparent myocardium/blood pool contrast and CNR have increased, the clinical significance of these improvements in perfusion abnormality detection and diagnostic value of both LDD and FFD methods need to be investigated. In [41], Berman, et al. demonstrated that defect extent by visual and TPD is highly correlated, as it increases proportionally to the degree of ischemia. In other studies, investigators also found a strong similarity between visual TPD in CT-MPI with automatically derived TPD in SPECT-MPI [42]. Hence, studying TPD is of great importance to us, and the TPD results presented in Fig. 4 show that TPD-LDD is in good agreement with TPD-MF algorithm and have no statistically significant difference (p = 0.13), which might indicate similar diagnostic value of these approaches.

5. Conclusion

In this study we have investigated the efficiency of three different contraction motion compensation approaches in gated myocardial perfusion SPECT (MPS), one of which is a routine clinical application (MF) for MPS image analyses. All methods were used retrospectively and significantly reduced motion induced blurring, while keeping SNR and mean count density intact. LDD and FFD are fully automatic and do

not require any manual intervention, whereas

MF is dependent on contour definition, which is strongly dependent on operator's expertise, and the contour definition accuracy affects image display and further quantifications. Image quality analysis results indicated an improvement in image quality after motion compensation. LDD and FFD assume image intensity a consistent feature in subsequent frames, although it might be influenced by the partial volume effect in systolic frames. However, MF warps images using geometric control points and the image intensity is not a prominent factor in registration process. Thus, FFD and LDD, illustrated similar results in terms of M/BP contrast and CNR, while MF shows the greatest impact on these parameters. Lateral wall thickness after motion compensation is reduced with respect to corresponding NoMC images (p < 0.0001). TPD-LDD and TPD-MF are in good agreement, which indicates that these both techniques might be in line in terms of clinical parameters. Further investigation including diagnostic reference standards is required in order to definitively evaluate the actual clinical utility of the respective motion compensation methods in myocardial perfusion imaging.

Acknowledgments

References

[1] Hansen CL, Goldstein RA, Akinboboye OO, Berman DS, Botvinick EH, Churchwell KB, et al. Myocardial perfusion and function: single photon emission computed tomography. J Nucl Cardiol: Official Publ Am Soc Nucl Cardiol 2007;14:e39–60.

[2] Dawood M, Buther F, Jiang X, Schafers KP. Respiratory motion correction in 3-D PET data with advanced optical flow algorithms. IEEE Trans Med Imaging 2008;27:1164–75.

[3] Gigengack F, Ruthotto L, Burger M, Wolters CH, Jiang X, Sch K, et al. Motion correction of cardiac PET using mass-preserving registration. In: IEEE Nuclear Science Symposuim & Medical Imaging Conference 2010. p. 3317–9.

[4] Rahmim A, Tang J, Zaidi H. Four-dimensional image reconstruction strategies in cardiac-gated and respiratory-gated PET imaging. PET Clinics 2013;8:51–67.

[5] Kovalski G, Israel O, Keidar Z, Frenkel A, Sachs J, Azhari H. Correction of heart motion due to respiration in clinical myocardial perfusion SPECT scans using respiratory gating. J Nucl Med : Official Publ, Soc Nucl Med 2007;48:630–6.

[6] Kovalski G, Keidar Z, Frenkel A, Sachs J, Attia S, Azhari H. Dual, "motion-frozen heart" combining respiration and contraction compensation in clinical myocardial perfusion SPECT imaging. J Nucl Cardiol: Official Publ Am Soc Nucl Cardiol 2009;16:396–404.

[7] Slomka PJ, Nishina H, Berman DS, Kang X, Akincioglu C, Friedman JD, et al. "Motion-frozen" display and quantification of myocardial perfusion. J Nucl Med 2004;45:1128–34.

[8] Chandra R, Rahmim A. 8th ed. Nuclear medicine physics: the basics Philadelphia, PA: Wolters Kluwer; 2017.

[9] Holly T, Abbott B, Al-Mallah M, Calnon D, Cohen M, DiFilippo F. ASNC imaging guidelines for nuclear cardiology procedures. Single photon-emission computed tomography. 2010. 2011.

[10] Taillefer R, DePuey EG, Udelson JE, Beller GA, Benjamin C, Gagnon A. Comparison between the end-diastolic images and the summed images of gated 99mTc-sesta-mibi SPECT perfusion study in detection of coronary artery disease in women. J Nucl Cardiol: Official Publ Am Soc Nucl Cardiol 1999;6:169–76.

[11] Petibon Y, Ouyang J, Zhu X, Huang C, Reese TG, Chun SY, et al. Cardiac motion compensation and resolution modeling in simultaneous PET-MR: a cardiac lesion detection study. Phys Med Biol 2013;58:2085–102.

[12] Feng T, Wang J, Fung G, Tsui B. Non-rigid dual respiratory and cardiac motion correction methods after, during, and before image reconstruction for 4D cardiac PET. Phys Med Biol 2016;61:151–68.

[13] Klein G, Reutter B, Huesman R. Non-rigid summing of gated PET via optical flow. IEEE Trans Nucl Sci 1997;44:1509–12.

[14] Mair BA, Gilland DR, Cao Z. Simultaneous motion estimation and image reconstruction from gated data. Biomedical Imaging. In: 2002 Proceedings 2002 IEEE International Symposium on: IEEE; 2002. p. 661–4.

[15] Marin T, Wernick MN, Yang Y, Brankov JG. Motion-compensated temporal summation of cardiac gated SPECT images using a deformable mesh model. In: Conference proceedings: Annual International Conference of the IEEE Engineering in Medicine and Biology Society IEEE Engineering in Medicine and Biology Society Annual Conference. 2009;2009:3657-60.

[16] Marin T, Wernick MN, Yang Y, Brankov JG. Motion-compensated temporal summation of cardiac gated SPECT images using a deformable mesh model. In: Conference proceedings: Annual International Conference of the IEEE Engineering

[17] Marin T, Wernick MN, Yang Y, Brankov JG. Motion-compensated reconstruction of gated cardiac SPECT images using a deformable mesh model. In: 2010 IEEE International Symposium on Biomedical Imaging: From Nano to Macro 2010. p. 520–3.

[18] O'Dell WGMCC, Hunter WC, Zerhouni EA, McVeigh ER. Three-dimensional myocardial deformations: calculation with displacement field fitting to taggedMR images. Radiology 1995;195:829–35.

[19] Rahmim A, Rousset OG, Zaidi H. Strategies for motion tracking and correction in PET. PET Clinics 2007;2:251–66.

[20] Qiao F, Pan T, Clark Jr. JW, Mawlawi OR. A motion-incorporated reconstruction method for gated PET studies. Phys Med Biol 2006;51:3769–83.

[21] Li T, Thorndyke B, Schreibmann E, Yang Y, Xing L. Model-based image reconstruction for four-dimensional PET. Med Phys 2006;33:1288–98.

[22] Germano G, Kavanagh PB, Chen J, Waechter P, Su H-T, Kiat H, et al. Operator-less processing of myocardial perfusion SPECT studies. J Nucl Med 1995;36:2127–32.

[23] Khare R, Sala G, Kinahan P, Esposito G, Banovac F, Cleary K, et al. Experimental evaluation of a deformable registration algorithm for motion correction in PET-CT guided biopsy. In: 2013 IEEE Nuclear Science Symposium and Medical Imaging Conference (2013 NSS/MIC)2013. p. 1–5.

[24] Vercauteren T, Pennec X, Perchant A, Ayache N. Symmetric log-domain diffeomorphic registration: A demons-based approach. Medical Image Computing and Computer-Assisted Intervention–MICCAI 2008: Springer; 2008. p. 754–61.

[25] Beg MF, Miller MI, Trouvé A, Younes L. Computing large deformation metric mappings via geodesic flows of diffeomorphisms. Int J Comput Vision 2005;61:139–57.

[26] McLeod K, Prakosa A, Mansi T, Sermesant M, Pennec X. An incompressible log-domain demons algorithm for tracking heart tissue. International Workshop on Statistical Atlases and Computational Models of the Heart Springer; 2011. p. 55–67.

[27] Rueckert D, Sonoda LI, Hayes C, Hill DL, Leach MO, Hawkes DJ. Nonrigid registration using free-form deformations: application to breast MR images. IEEE Trans Med Imaging 1999;18:712–21.

[28] Shen J-K, Matuszewski BJ, Shark L-K, Skalski A, Zielinski T, Moore CJ. Deformable image registration-A critical evaluation: Demons, b-spline FFD and spring mass system. In: BioMedical Visualization, 2008 MEDIVIS'08 Fifth International Conference: IEEE; 2008. p. 77–82.

[29] Wang H, Gong G, Wang H, Li D, Yin Y, Lu J. Performance evaluations of demons and free form deformation algorithms for the liver region. Technol Cancer Res Treat 2014;13:101–8.

[30] Rubeaux M, Joshi N, Dweck MR, Fletcher A, Motwani M, Thomson LE, et al. Demons versus Level-Set motion registration for coronary (18)F-sodium fluoride PET. In: Proceedings of SPIE–the International Society for Optical Engineering. 2016;9784:97843Y.

[31] Slomka PJ, Rubeaux M, Le Meunier L, Dey D, Lazewatsky JL, Pan T, et al. Dual-Gated Motion-Frozen Cardiac PET with Flurpiridaz F 18. J Nucl Med: Official Publ, Soc Nucl Med 2015;56:1876–81.

[32] Dawood M, Gigengack F, Jiang X, Schafers KP. A mass conservation-based optical flow method for cardiac motion correction in 3D-PET. Med Phys 2013;40:012505.

[33] Suzuki Y, Slomka PJ, Wolak A, Ohba M, Suzuki S, De Yang L, et al. "Motion-frozen" myocardial perfusion spect improves detection of coronary artery disease in obese patients. J Nucl Med: Official Publ, Soc Nucl Med 2008;49:1075–9.

[34] Bookstein FL. Principal warps: thin-plate splines and the decomposition of deformations. IEEE Trans Pattern Anal Mach Intell 1989;11:567–85.

[35] Xin H, Zhu Y, Wu L. A comparative study of adaptive registration methods for two dimensional gel electrophoresis images. In: Conference proceedings: Annual International Conference of the IEEE Engineering in Medicine and Biology Society IEEE Engineering in Medicine and Biology Society Annual Conference. 2007;2007:6240-3.

[36] Mansi T, Pennec X, Sermesant M, Delingette H, Ayache N. ILogDemons: a demons-based registration algorithm for tracking incompressible elastic biological tissues. Int J Comput Vision 2011;92:92–111.

[37] Dawant BM. Non-rigid registration of medical images: purpose and methods, a short survey. In: 2002 Proceedings 2002 IEEE International Symposium on Biomedical Imaging: IEEE; 2002. p. 465–8.

[38] Sotiras A, Davatzikos C, Paragios N. Deformable medical image registration: a survey. IEEE Trans Med Imaging 2013;32:1153–90.

[39] Salehi N, Fatemizadeh E, Farahani MH, Akbarzadeh A, Farzanehfar S, reza Ay M. Cardiac Contraction Motion Correction in Gated Myocardial Perfusion SPECT Projection Domain. Frontiers in Biomedical Technologies. 2017;2:206–13.

[40] Dawood M, Brune C, Jiang X, Büther F, Burger M, Schober O, et al. A Continuity Equation Based Optical Flow Method for Cardiac Motion Correction in 3D PET Data. In: Liao H, Edwards PJE, Pan X, Fan Y, Yang G-Z, editors. Medical Imaging and Augmented Reality: 5th International Workshop, MIAR 2010, Beijing, China, September 19-20, 2010 Proceedings. Berlin, Heidelberg: Springer Berlin Heidelberg; 2010. p. 88-97.

[41] Berman DS, Kang X, Gransar H, Gerlach J, Friedman JD, Hayes SW, et al. Quantitative assessment of myocardial perfusion abnormality on SPECT myocardial perfusion imaging is more reproducible than expert visual analysis. J Nucl Cardiol: Official Publ Am Soc Nucl Cardiol 2009;16:45–53.

[42] Tamarappoo BK, Dey D, Nakazato R, Shmilovich H, Smith T, Cheng VY, et al. Comparison of the extent and severity of myocardial perfusion defects measured by CT coronary angiography and SPECT myocardial perfusion imaging. JACC: Cardiovascular Imaging 2010;3:1010–9.